Bright Unidirectional Fluorescence Emission of Molecules in a Nanoaperture with Plasmonic Corrugations

Heykel Aouani,[†] Oussama Mahboub,[‡] Nicolas Bonod,[†] Eloïse Devaux,[‡] Evgeny Popov,[†] Hervé Rigneault,[†] Thomas W. Ebbesen,[‡] and Jérôme Wenger*,[†]

[†]Institut Fresnel, Aix-Marseille Université, CNRS, Ecole Centrale Marseille, Campus de St Jérôme, 13397 Marseille, France
[‡]Institut de Science et d'Ingénierie Supramoléculaires, Université de Strasbourg, CNRS, 8 allée G. Monge, 67000 Strasbourg, France

Ⓢ *Supporting Information*

ABSTRACT: Controlling the fluorescence emission from nanoscale quantum emitters is a key element for a wide range of applications, from efficient analytical sensing to quantum information processing. Enhancing the fluorescence intensity and narrowing the emission directivity are both essential features to achieve a full control of fluorescence, yet this is rarely obtained simultaneously with optical nanoantennas. Here we report that gold nanoapertures surrounded by periodic corrugations transform standard fluorescent molecules into bright unidirectional sources. We obtain enhancement factors of the fluorescence count rate per molecule up to 120 fold simultaneously with a directional emission of the fluorescence into a narrow angular cone in the

direction normal to the sample plane. The bright emission and narrow directionality enable the detection of single molecules with a low numerical aperture objective, and improve the effectiveness of fluorescence-based applications. We thoroughly quantify the increased light-matter coupling as well as the radiation pattern intensity. These results are highly relevant for the development of single molecule sensing, single-photon sources, and light emitting devices.

KEYWORDS: Plasmonics, nanoantennas, metal nanoapertures, fluorescence enhancement, fluorescence correlation spectroscopy, nanofabrication
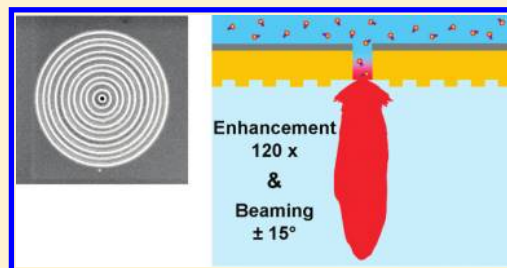
Efficiently detecting the generally weak fluorescence signal emitted by a single molecule is of great interest due to the widespread use of fluorescence-based techniques in chemistry, molecular biology, materials science, and medicine.[1,2] For instance, applications on DNA sequencing, early diagnosis, or drug screening directly rely on the detected signal per molecule.[3] To overcome the detection limits set by the optical diffraction phenomenon, the environment surrounding the molecule can be tailored to control both the fluorescence intensity and the angular radiation pattern.[4] This leads to the concept of optical antennas, which reversibly convert the propagating optical energy into localized energy in nanoscale volumes, and are the counterparts of radio and microwave antennas in the optical regime.[5] Optical antennas provide new conceptual routes to locally enhance and direct the electromagnetic fields with major applications in molecular sensing and spectroscopy,[6] light-emitting devices,[7] and photovoltaics.[8]

To improve the detection of single molecules using optical antennas, both the antenna's enhancement factor and directivity are essential characteristics. The enhancement denotes the ability to locally increase the fluorescence count rate and the light-matter interaction, while the directivity measures the ability to concentrate the radiated power into a certain direction.[5] The enhancement aspect has received a considerable interest, mainly

driven by the opportunity of improving the efficiencies of biomolecular sensing and spectroscopies.[2,6,9,10] The directivity aspect of optical nanoantennas has received much less experimental attention until very recently,[11] owing to the difficulty to realize plasmonic structures achieving directional control of the radiation from single quantum emitters.[12−16] Both enhancement factor and directivity of nanoantennas are essential features for the improvement of light-matter interaction and its wide applications. However, to the best of our knowledge there is no clear demonstration of nanoantennas to improve the fluorescence count rates per molecule and simultaneously provide directional control on the emission. There is currently a strong demand for experimental realizations of nanoantennas able to reach simultaneously a strong gain in the fluorescence signal, together with a unidirectional emission into a narrow angular cone.

In this Letter, we report the demonstration of bright unidirectional photon sources from fluorescent molecules. We obtain enhancement factors of the fluorescence count rate per molecule up to 120 fold, simultaneously with a directional emission of the fluorescence into a cone of ±15° in the direction normal to the
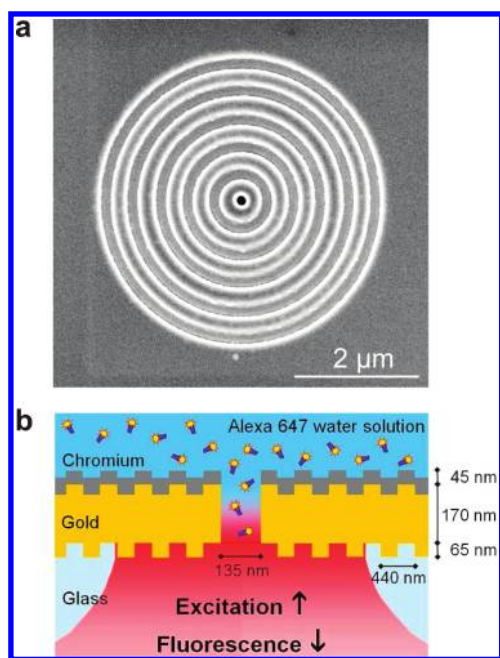
Figure 1. (a) Scanning electron microscopy image of the fabricated nanoaperture with five corrugations. (b) Configuration to enhance and control the fluorescence emission of molecules diffusing in the central aperture.

sample plane. To achieve this, we couple fluorescent molecules to a single nanoaperture surrounded by periodic corrugations milled in a thick gold film (Figure 1). The periodic circular corrugations act as a grating antenna to reversibly couple light to surface electromagnetic waves, as pioneered by Lezec and co-workers while studying the transmission of light through a single subwavelength aperture.[17] All measured signals are calculated back to average signal per molecule thanks to a calibration of the average number of molecules in the central nanoaperture by fluorescence correlation spectroscopy (FCS).

Nanoapertures surrounded by periodic corrugations (also known as "bull's eyes" apertures) have received a considerable interest in the photonics community.[18,19] Much higher transmission can be achieved through these corrugated apertures than with standard noncorrugated apertures.[20] Moreover, if the output surface surrounding the aperture is also corrugated, a surprisingly narrow beam can be transmitted, having a divergence of less than a few degrees, which is far smaller than that of a simple aperture.[17] The antenna capacity of the corrugations to concentrate the photons at the tiny central aperture has also been used to realize novel applications in nonlinear optics,[21] ultrafast detectors,[22] optical data storage and nanolithography,[23] optical filters and sorters,[24] and semiconductor lasers.[25] The present study explores the use of corrugated nanoapertures for fluorescence sensing applications. This is the first study where single apertures surrounded by periodic corrugations are used to enhance the fluorescence count rate of molecules and control the emission directionality. The results are of high importance to improve the effectiveness of single molecule fluorescence detection[26,27] with applications in molecular sensing,[28,29] DNA sequencing,[30,31] high throughput screening,[32] or optical trapping.[33]

The average number of fluorescent molecules can be more than 2 orders of magnitude smaller in a nanoaperture than in a diffraction-limited classical confocal volume.[34] Therefore, the

sole measurement of the total fluorescence intensity from the sample is not sufficient to accurately quantify the antennas properties of enhancement factor and directivity. The fluorescence intensity has to be normalized by the number of emitters that actually contribute to the signal to assess the fluorescence count rate per molecule CRM, which is the relevant figure to assess the enhancement on the fluorescence signal. We address this issue using FCS, which is an elegant method to directly and accurately quantify the average number of emitters N contributing to the detected fluorescence signal.[34,35] In FCS, the temporal fluctuations of the fluorescence signal $F(t)$ are recorded, and the temporal correlation of this signal is computed $g^{(2)}(\tau) = \langle F(t)F(t+\tau)\rangle/\langle F(t)\rangle^2$, where τ is the delay (lag) time, and $\langle\ \rangle$ stands for time averaging. The amplitude of the correlation function quantifies the average number of molecules N and provides access to the fluorescence count rate per molecule CRM $= \langle F\rangle/N$. Full details of the FCS analysis procedure are given in the Supporting Information, together with raw experimental FCS data. We point out that as a consequence of the stochastic nature of the FCS technique, all the presented fluorescence data are spatially averaged over all the possible molecule orientations and positions inside the detection volume. While FCS is not a "true" single molecule method, it nevertheless quantifies the average fluorescence emission characteristics of a single emitter. Hereafter, we use the FCS method to characterize the fluorescence emission per Alexa Fluor 647 molecules diffusing within the central nanoaperture. The emission count rate per molecule is the key to thoroughly analyze the fluorescence enhancement and the angular radiation pattern molecules in corrugated nanoapertures. Moreover, the method is able to specifically quantify the respective contributions of excitation and emission processes in the observed enhanced fluorescence.[35,36] We demonstrate that the periodic corrugations improve the local excitation intensity inside the central nanoaperture, while simultaneously increasing the directional emission count rate.

Figure 1 presents the doubly corrugated nanoapertures under investigation. The different nanostructures are fabricated by direct focused ion beam (FIB) milling, using optimized design parameters derived from the thorough characterization published in ref 37. The fabrication protocol is detailed in the Supporting Information. The inner aperture diameter is 135 nm and is chosen to be close to the optimum diameter leading to maximum fluorescence enhancement.[38] The groove period is 440 nm, width 200 nm, depth 65 nm, and there are 5 grooves. The periodic grooves provide the necessary momentum to match the far-field radiation with surface electromagnetic waves. As the Stokes shift between the laser and the fluorescence wavelengths is relatively small, these design parameters can be sufficiently close to resonance conditions for both the laser excitation and the fluorescence emission.[37] A spectral study shown in the Supporting Information does not reveal any major spectral resonance effect.

An unwanted phenomenon consecutive to the use of periodic corrugations on both sides of the gold film is the enhanced transmission through the central aperture.[17] Even the fluorescence from molecules diffusing above the nanoaperture could be detected, which would confuse the analysis. To solve this problem, we cover the gold film with an optically thick (45 nm) chromium layer, following the investigations in reference[39] on bowties nanoantennas. The high absorption losses of chromium efficiently damp the transmission through the corrugated nanoaperture and avoid detecting a fluorescence signal from the top of the nanoaperture sample. We demonstrate in the Supporting
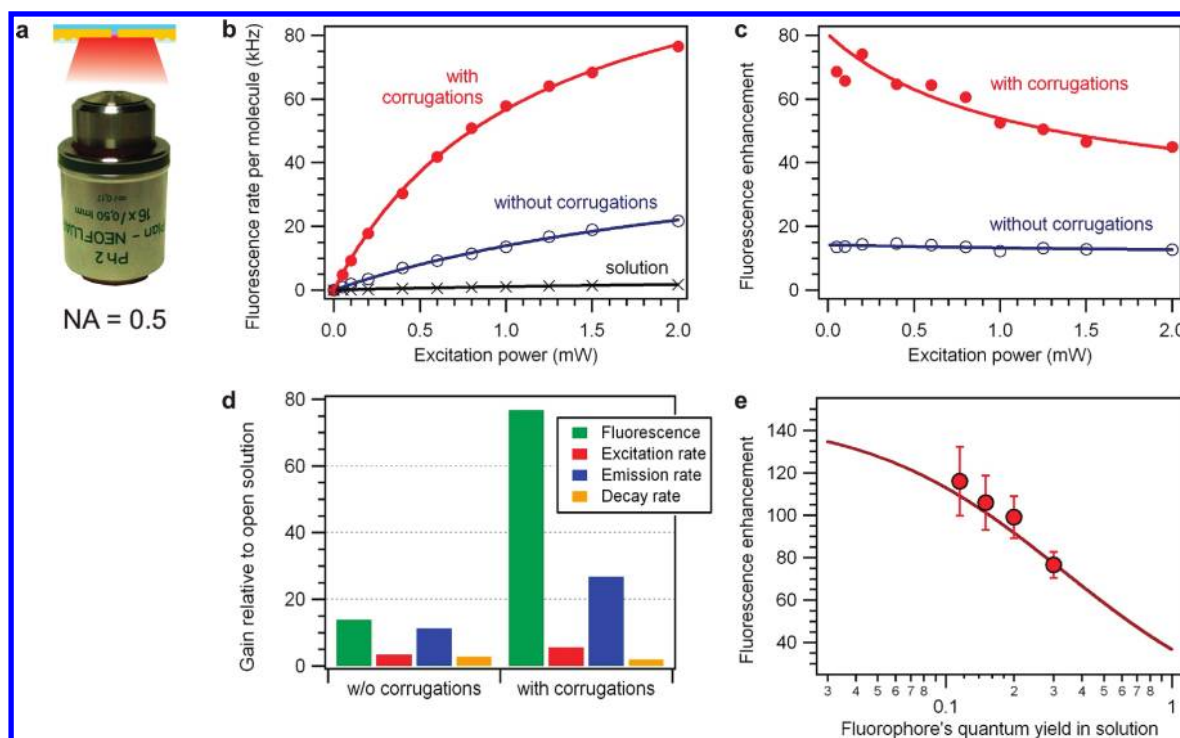
Figure 2. (a) Investigations of the detected fluorescence count rate per molecule with a 0.5 NA water immersion microscope objective. (b) Fluorescence count rate per molecule versus the excitation power. Markers are experimental data, solid lines are numerical fits using a model detailed in the main text. The fitting parameters are summarized in the Supporting Information. (c) Fluorescence enhancement factors relative to the standard confocal case (open solution), as deduced from the data in (b). (d) Contribution of excitation and emission gains to the overall fluorescence enhancement. Decay rate corresponds to the reduction of the fluorescence lifetime. The experimental values are summarized in the main text. (e) Evolution of the fluorescence enhancement factor versus Alexa Fluor 647 measured quantum yield ϕ in a water-methyl viologen solution. From right to left, the methyl viologen concentration increases from 0 up to 60 mM. The continuous line is a model based solely on the data displayed in (d). It is not a numerical fit of the experimental data points, there are no free parameters.

Information that similar numbers of molecules are detected for nanoapertures with and without corrugations thanks to the supplementary chromium layer. Without the chromium layer, the difference in the numbers of molecules can be larger than a factor of 6 fold.

The excitation is incident from below the sample (glass coverslip substrate) with linear polarization and 632.8 nm wavelength. It is focused by a 0.5 NA water-immersion objective (Zeiss Neofluar, see Figure 2a) to a spot diameter of about 1.5 μm largely covering the first three concentric corrugations. The same microscope objective is used to collect the fluorescence light emitted from Alexa Fluor 647 molecules (A647, Invitrogen, Carlsbad, CA) diffusing in the central aperture region. Alexa Fluor 647 is a common fluorescent molecule with maximum absorption/emission peaks at 650/672 nm, and a quantum yield of 30% in water solution. Unless otherwise stated, A647 molecules are diluted in a standard water-based phosphate-buffered saline (PBS) solution. The salt composition of the PBS buffer is expected to compensate for the local electrical charging of the nanoaperture surface acquired during the FIB fabrication process. For all the experiments reported here, a solution of A647 molecules at micromolar concentration is deposited on top of the sample to ensure that on average 10 molecules are present in the aperture volume, as calibrated by FCS for each experimental run (see the raw experimental data in the Supporting Information). The molecules are constantly diffusing in and out the aperture, this configuration strongly limits observing the negative effects of photobleaching in our data set.

The fluorescence count rates per molecule measured by FCS are plotted as function of the excitation power in Figure 2b for the three cases of (i) free solution (no nanostructure), (ii) gold nanoaperture without corrugations, and (iii) gold nanoaperture with the periodic corrugations. It is apparent from this set of data that the periodic corrugations have a strong influence in further enhancing the fluorescence emission. The experimental points are numerically fitted following the general model of the fluorescence count rate CRM = $AI_e/(1 + I_e/I_s)$, where I_e is the excitation power, I_s the saturation power, and A is a constant proportional to the molecular absorption cross-section, quantum yield, and setup collection efficiency.[35] The fitting parameters are summarized in the Supporting Information and will be used hereafter to quantify the influence of excitation and emission gains in the fluorescence enhancement process.

These measurements unambiguously quantify the enhancement of the fluorescence intensity, which is the first essential feature of the nanoantenna. We define the fluorescence enhancement factor η_F as the direct ratio of the fluorescence count rates per molecule for the nanostructure and the reference (open) solution at a given excitation power: $\eta_F = $ CRM$_{aper}$/CRM$_{sol}$. Figure 2c presents a clear evolution of the fluorescence enhancement factor with the excitation power. For both apertures with and without corrugations, the enhancement η_F decreases with the excitation power, as the fluorescence process tends to saturate.[35] In the low excitation regime ($I_e < 200$ μW), the corrugated nanoaperture provides a enhancement factor of $\eta_F = 77$, while the enhancement factor of the noncorrugated nanoa-

perture is 14. Adding plasmonic corrugations enables achieving close to 2 orders of magnitude enhancement factor, while using a standard fluorophore. Compared to the use of a noncorrugated aperture, the corrugations provide a supplementary gain of 5.5. These measurements also demonstrate that single molecule fluorescence analysis can be efficiently performed by a simple 0.5 NA water immersion objective, or equivalently 0.4 NA dry air objective.

The evolution of the fluorescence enhancement versus the excitation power (Figure 2c) allows to quantify the respective contributions of excitation and emission gains and unravel the origins of the fluorescence enhancement following a procedure developed in references.[35,36] From the interpolation of the fluorescence count rates per molecule CRM versus the excitation power, we deduce the fluorescence enhancements at the two extreme cases below saturation $I_e \ll I_s$ and at saturation $I_e \gg I_s$. In the asymptotic limit of the saturation regime, the fluorescence enhancement corresponds to the gain in emission η_{em}, as there is obviously no dependence anymore on the excitation power. The emission enhancement η_{em} can be expressed as the product of the radiative rate enhancement η_{rad} times the collection efficiency enhancement η_κ, $\eta_{em} = \eta_{rad}\eta_\kappa$. While most numerical simulations focus on the radiative rate enhancement, the experimental characterization procedure is only sensitive to the photons that are collected by the setup, and accesses to the product of the radiative decay rate k_r times the collection efficiency κ. In the low excitation regime $I_e \ll I_s$, the fluorescence enhancement η_F is proportional to the gains in emission η_{em} and local excitation intensity η_{exc}, and inversely proportional to the modification in total fluorescence decay rate η_{tot}, $\eta_F = \eta_{em}\eta_{exc}/\eta_{tot}$.[5] This expression can be rewritten as $\eta_F = \eta_\kappa\eta_\phi\eta_{exc}$, where η_κ is the collection efficiency enhancement, and $\eta_\phi = \eta_{rad}/\eta_{tot}$ is the quantum efficiency enhancement. This expression of the fluorescence enhancement explicitly indicates that in the low excitation regime, the fluorescence enhancement is proportional to the gains in collection efficiency, quantum yield, and excitation intensity. We determine experimentally the alteration in the total fluorescence decay rate η_{tot} by fluorescence lifetime (start−stop) measurements. We can thus extract the gain in local excitation intensity from the fluorescence enhancement in the low excitation regime, knowing η_{tot} and η_{em} (the latter corresponds to the fluorescence enhancement factor in the saturation regime). This procedure separates the excitation and emission contributions from the total fluorescence enhancement and is used here to investigate the influence of the periodic corrugations surrounding single nanoapertures.

The periodic grating structure acts as an antenna to reversibly couple far-field light radiation to near-field electromagnetic energy. Our characterization procedure is able to quantify this effect clearly, as shown in Figure 2d. For the nanoaperture without corrugations, we measure the different enhancement factors relative to the reference in open solution (no aperture): total fluorescence $\eta_F = 14$, excitation $\eta_{exc} = 3.2$, emission $\eta_{em} = 11$, and total decay rate $\eta_{tot} = 2.5$ (this increase in total decay rate corresponds to the reduction of the fluorescence lifetime). These values stand in good agreement with the values previously reported from FCS measurements[35] or from quantum dot photoluminescence dynamics.[40] For the corrugated nanoaperture, we find that the enhancement factors are significantly greater: fluorescence $\eta_F = 77$, excitation $\eta_{exc} = 5.5$, emission $\eta_{em} = 27$, while the total decay rate modification is almost unchanged $\eta_{tot} = 1.9$. Here again, the values for the excitation and

emission correspond well to what can be inferred from transmission measurements and simulations on corrugated nanoapertures.[17,20] We note that the emission enhancement η_{em} is always larger than the excitation enhancement η_{exc}. This is because the emission enhancement is the product of the radiative rate enhancement η_{rad} times the collection efficiency enhancement η_κ. By reciprocity, we expect the radiative rate enhancement η_{rad} to be close to the excitation enhancement η_{exc}.[41] Consequently, the emission enhancement η_{em} is larger than the excitation enhancement η_{exc} by a factor that is close to the collection efficiency enhancement η_κ.

The characterization of the fluorescence enhancement shows that (i) both excitation and emission gains contribute to the overall fluorescence enhancement, and (ii) the periodic corrugations increase each gain in excitation and emission by roughly a factor of 2, as compared to a nanoaperture without corrugations. The grating structure acts as an antenna to concentrate the photons at the central nanoaperture with an increase in excitation intensity from 3.2 to 5.5 fold. The periodic corrugations also reversibly couple the near-field electromagnetic energy into far-field light radiation, with an gain in emission count rate from 11 to 27 fold. The simultaneous increase in both η_{exc} and η_{em} is permitted by the Stokes shift between the laser and the fluorescence wavelengths remaining on the order of $\lambda/20$. The periodic corrugations can thus be close to resonance conditions for both the laser excitation and the fluorescence emission.

The fluorescence enhancement factor obviously depends strongly on the fluorophore's quantum yield in solution; for a perfect emitter (quantum yield of one), all the fluorescence enhancement comes from the excitation intensity or collection efficiency, as there is no possible gain on the quantum yield. The lower the quantum yield in solution, the higher the gain on a plasmonic nanostructure can be, up to a certain extend where the losses are going to limit the enhancement factor.[42] To illustrate this, remarkably large single molecule fluorescence enhancements up to 1340 have been reported while studying TDQPI molecules.[10] These nonwater-soluble molecules have a relatively low quantum yield of ∼2.5%, which can be favorable to obtain large enhancement values. Here, we experimentally address the evolution of the fluorescence enhancement factor versus the fluorophore's quantum yield in solution. To control the A647 quantum yield, we add a growing fraction of methyl viologen (1,1′-dimethyl-4,4′-bipyridinium dichloride, Sigma-Aldrich) with concentrations up to 60 mM. Methyl viologen acts as a controllable quencher of the A647 fluorescence. A Stern−Volmer analysis shown in the Supporting Information quantifies this effect: in the presence of methyl viologen with concentration $[MV^{2+}]$, the quantum yield ϕ of A647 is decreased according to the formula $\phi_0/\phi = 1 + k_q \tau_0 [MV^{2+}]$, where $\phi_0 = 30\%$ and $\tau_0 = 1.0$ ns are the unquenched quantum yield and fluorescence lifetime of A647 in water PBS solution, and $k_q = 2.4 \times 10^{10} \text{ s}^{-1} \cdot \text{M}^{-1}$ is the quenching rate determined experimentally (see Supporting Information).

The A647 and methyl viologen mixture forms the ideal basis to check the evolution of the fluorescence enhancement factor while varying the initial quantum yield in solution. Our results are summarized in Figure 2e, showing a net increase in the fluorescence enhancement factor from 77 to 120 while the A647 quantum yield is quenched from 30 to 11% (added methyl viologen concentration up to 60 mM). This experimental data is analyzed using only the enhancement factors in Figure 2d, which we detail hereafter. Without the nanostructure, the fluorescent

molecule has a radiative decay rate k_r, a nonradiative decay rate $k_{nr_0} + k_q$ [MV^{2+}], and a quantum yield $\phi = k_r/(k_r + k_{nr_0} + k_q$ [MV^{2+}]). The setup collection efficiency is κ and the excitation rate is k_e. With the introduction of the nanostructure, the radiative rate is modified to k_r^*, the collection efficiency is κ^*, and the excitation rate k_e^*. The quantum yield now reads $\phi^* = k_r^*/(k_r^* + k_{nr_0} + k_q$ [MV^{2+}] $+ k_{abs}^*)$, where a new nonradiative decay route k_{abs}^* is introduced to take into account the ohmic losses into the metal and nonradiative energy transfers to the free electrons in the metal.[10] We also assume that the rates k_{nr_0} and k_q are unaffected by the nanostructure. At moderate excitation powers (below fluorescence saturation), the fluorescence count rate per molecule CRM is proportional to the excitation rate k_e, the collection efficiency κ, and the emission quantum yield ϕ.[35] The fluorescence enhancement with the nanoaperture can thus be explicitly written as

$$\eta_F = \frac{k_e^*}{k_e} \frac{\kappa^*}{\kappa} \frac{\phi^*}{\phi} \qquad (1)$$

After some basic algebra, this equation can be rewritten:

$$\eta_F = \frac{k_e^*}{k_e} \frac{\kappa^*}{\kappa} \frac{k_r^*}{k_r} \frac{1}{(1-\phi)+\phi\zeta} = \eta_{exc}\eta_{em}\frac{1}{(1-\phi)+\phi\zeta} \qquad (2)$$

with $\zeta = (k_r^* + k_{abs}^*)/k_r$. Hereafter, we set the quantity ζ to the value obtained from the characterization of A647 with no methyl viologen (Figure 2d). The linear curve in Figure 2e displays the awaited fluorescence enhancement factors η_F while varying the quantum yield in solution ϕ based on eq 2. Let us emphasize that this is not a numerical fit of the experimental data points, as there are no free parameters. This curve is only based on the values of the gains in excitation, emission, and total decay rates as deduced from the fluorescence characterization of A647 with no methyl viologen (Figure 2d). The satisfactorily agreement with the data points in Figure 2e is another confirmation of the validity of the fluorescence characterization procedure (see more characterization with a 1.2 NA objective in the Supporting Information). Besides, the theoretical predictions indicate that no fluorescence enhancement factor higher than 150 could be reached with this experimental configuration, whatever the choice of the fluorophore's quantum yield in solution. Further reducing the aperture diameter is not expected to significantly improve the fluorescence enhancement, as the diameter of 135 nm is already close to the optimum diameter leading to maximum enhancement for a non-corrugated aperture, independently on the fluorophore's quantum yield in solution.[43] Higher enhancement values seem restricted to plasmonic nanoantennas with higher electromagnetic field confinement and lightning rod effect, such as bowties nanoantennas,[10] which is not surprising at all. However, the corrugated nanoapertures have another crucial advantage, which deals with the ability to control the fluorescence emission directivity.

After the fluorescence enhancement parameter, the second essential feature of the nanoaperture antenna is the directivity, which measures the antenna's ability to concentrate the radiated power into a certain direction. To characterize the directivity of the corrugated nanoaperture, we switch the microscope objective to a 1.2 NA water immersion objective (Zeiss C-apochromat). This is essential to provide enough range for the angular detection, with a present detection limit set by the numerical aperture to ±64° around the optical axis. To characterize the angular emission, we record the fluorescence intensity distribution on the back focal plane of the high NA microscope objective

on a charge-coupled device CCD camera with microlenses (Kodak KAF-1603).[44] These images represent the intensity emitted for different angular directions from the antenna, we call them radiation patterns (this corresponds formally to the emission diagram in the Fourier plane or equivalently the momentum space).[11] Typical radiation patterns for a single nanoaperture without and with periodic corrugations are presented in Figure 3a,b. Let us emphasize that as the FCS measurements provide an accurate estimation of the numbers of molecules N contributing to the overall fluorescence signal, we can normalize the intensities in the radiation pattern images by the actual number of molecules N for each experiment, which is the case in Figure 3. Therefore, the intensity scaling is to be understood as the normalized fluorescence per molecule. This is very important to provide an accurate picture of the radiation pattern and to be able to compare between different radiation patterns. Not only the shape of the radiation patterns in Figure 3 are important, the intensities are here fully relevant too.

For the noncorrugated aperture, the radiation pattern image contains a single circle representing the maximum collection angle at 64°. However, for the corrugated aperture, the image contains an additional bright spot with an extension of 15° (half-width at half-maximum) centered on the optical axis. This directly reveals that the emission from a noncorrugated aperture is almost omni-directional with no privileged direction, while the emission from the corrugated aperture can be tuned to high directionality in the direction normal to the sample. A first step to quantify the antenna's directionality is to introduce the "directional performance" as the ratio of the fluorescence intensity along the peak direction ($\theta = 0°$) relative to the fluorescence intensity emitted strongly off-axis (which we take at $\theta = 50°$ in the present case). For the noncorrugated aperture, the directional performance is roughly 0 dB, as expected for a subwavelength circular structure. For the corrugated aperture in Figure 3b, the directional performance is 7.3 dB, which appears similar to the performance of a recent Yagi-Uda antenna demonstration.[11] The periodic corrugations thus efficiently control the emission directionality. Moreover, the emission directionality is achieved along all azimuthal orientations (it is circularly symmetric in the back focal plane image), and the main emission direction is normal to the sample plane, contrarily to Yagi-Uda antennas.[11,45]

In antenna theory, "directivity" is a figure of merit for an antenna corresponding to the ratio of the radiated power density along the direction of strongest emission, relative to the power density radiated by an ideal isotropic emitter radiating the same amount of total power. As we quantify the radiation pattern intensity per molecule, we can estimate the directivity figure of merit and assess the fluorescence enhancement versus the emission angle. Figure 3c directly quantifies the fluorescence enhancement per molecule along each emission direction relative to an open water environment. To obtain this figure, we first calibrate the integrated fluorescence enhancement with the 1.2 NA objective in the case of the nanoaperture without corrugations. Data shown in the Supporting Information indicate an integrated value over the whole objective NA of 13.6. This value directly corresponds to the fluorescence enhancement found for each emission direction from a noncorrugated aperture, as the angular emission is uniform within the limit of ±64° set by our objective. In the case of the nanoaperture with the periodic corrugations, we use the ratio of the fluorescence intensities per molecule in Figure 3a,b and the known fluorescence
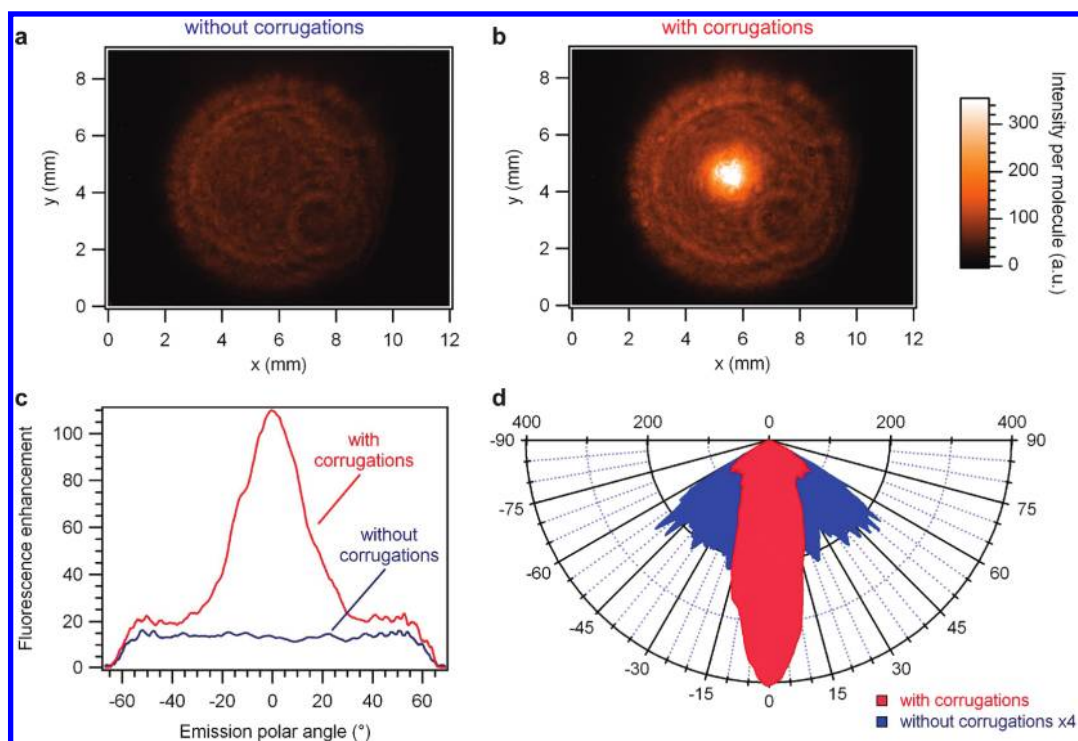
Figure 3. Radiation patterns (intensity distribution in the back focal plane of the 1.2 NA objective) for a single nanoaperture without (a) and with (b) periodic corrugations. The excitation power is 120 μW in both cases. The intensities presented here are normalized by the average number of detected molecules, as measured by FCS. Therefore, the intensity scaling in (a) and (b) corresponds to the normalized fluorescence intensity *per molecule*. The larger circle seen for instance in image (a) corresponds to the maximum detectable angle of $\pm64°$ set by our 1.2 NA water immersion objective. (c) Fluorescence intensity enhancement per single molecule as function of the emission polar angle, relative to the open solution reference case. (d) Angular radiation patterns in the polar angle, as deduced from the images in (a,b). The intensity per molecule in the case of the noncorrugated aperture is multiplied here by a factor of 4 to ease viewing the figure.

enhancement factor of 13.6 for an aperture without corrugations to calibrate the fluorescence enhancement versus the emission angle (Figure 3c). A clear peak centered at 0° (direction normal to the sample plane) is seen in Figure 3c with a peak enhancement up to 110 fold, or 20.5 dB. To quantify the antenna directivity, one needs to normalize this peak enhancement by the average enhancement integrated over all emission directions (directivity is defined relative to an isotropic source radiating the same total power). We estimate average enhancement integrated over all emission directions by the fluorescence enhancement of 23.8 found in the case of the 1.2 NA collection objective, divided by 2 to account for the emission occurring in the lower half-space only (see Supporting Information). As a result, the corrugated aperture directivity is estimated to $110/(23.8/2) = 9.2$, or equivalently 9.7 dB.

For the corrugated aperture, the peak seen in Figure 3c has a half-width at half-maximum of $\pm15°$, where most of the angular fluorescence enhancement is to be found. This value corresponds nicely to the $\pm22°$ collection cone of our 0.5 NA water-immersion objective. Almost all the energy of the central peak in the radiation pattern is thus collected by the 0.5 NA objective. This effect directly contributes to the high fluorescence enhancement found with the corrugated apertures, and to the ability to efficiently detect the fluorescence from a single molecule with a 0.5 NA objective. The radiation patterns are also shown in polar diagrams (Figure 3d), which are more intuitive to view. To complete this picture, the Supporting Information provides a comprehensive graph of the collected fluorescence per molecule versus the objective numerical aperture.

Lastly, we investigate the antenna capacity to couple the electromagnetic energy to the central aperture via surface electromagnetic waves. To this end, we perform the experiment depicted in Figure 4a; the fluorescence from the central aperture is measured while the excitation laser spot focused by a 1.2 NA water immersion objective is scanned over the corrugated nanoaperture sample. We emphasize that the fluorescence detection path is not scanned, only the emission from the fixed central aperture is collected while the excitation spot is moved. This type of image measurement directly notifies the occurrence of coupling through surface waves. It is also sensitive to the polarization coupling, as the laser light is linearly polarized and the corrugations grating has circular symmetry. Figure 4b,c represents the fluorescence images for horizontal and vertical polarization of the excitation field, while only the excitation spot is scanned over the corrugated nanoaperture. These pictures represent the direct image space (they must not be confused with radiation patterns in the reciprocal Fourier plane as in Figure 3a). The butterfly shape is characteristic to selective coupling when the field polarization is aligned along the transverse magnetic (TM) direction respective to the circular corrugations grating. This is directly representative of coupling to TM-sensitive surface waves such as surface plasmon polaritons. In the Supporting Information, we show an image scan of a single nanoaperture without corrugations. The characteristic butterfly shape is absent, as nothing (except the aperture edge) provides the necessary momentum to couple the far-field radiation to surface waves.

Gold nanoapertures surrounded by periodic corrugations transform standard fluorescent molecules into bright unidirectional
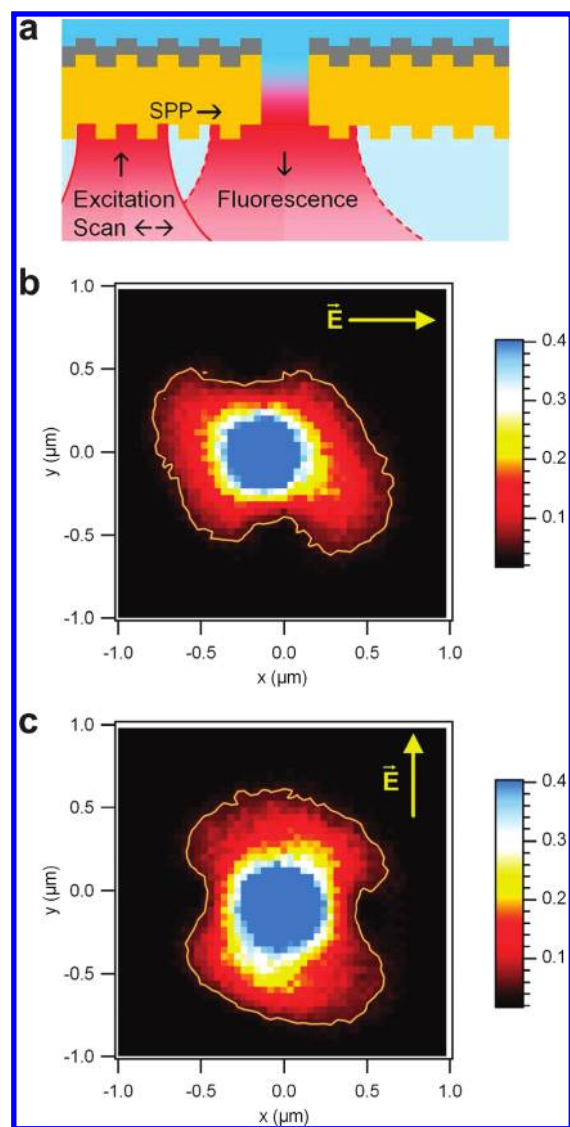
Figure 4. (a) Schematic of the experiment: the fluorescence from the central aperture is collected while the excitation laser spot focused by a 1.2 NA water immersion objective is scanned over the corrugated nanoaperture sample. The fluorescence detection path is not scanned, only the emission from the fixed central aperture is measured while the excitation spot is moved. (b,c) The fluorescence images for horizontal and vertical polarization of the excitation field. These pictures are in the direct image space (not reciprocal Fourier plane as in Figure 3a). We deliberately saturate the signal stemming from the center of the aperture (normalized to 1) to better display the intensity distribution near the periodic corrugations. The butterfly shape is characteristic to selective coupling when the field polarization is aligned along the transverse magnetic (TM) direction respective to the circular corrugations grating.

sources. The corrugated nanoaperture simultaneously increases the emission count rate and redirects the fluorescence radiation; our study reports enhancement factors of the fluorescence count rate per molecule up to 120 fold simultaneously with a directional emission of the fluorescence into a cone of ±15° in the direction normal to the sample. Corrugated nanoapertures thus provide a source for intense fluorescence light with very narrow directionality. There is still plenty of room for further optimization of the many antenna parameters, according to the design characterizations at hand.[37,46] On the basis of the very narrow directionality

of ±3° achieved for the transmitted light beam,[17] we believe that similar angular divergences can be realized for the fluorescence beam using optimized parameters design. Even though such directionality performance comes at the expense of a larger foot print of the structure, we point out that several corrugated apertures can be strongly overlapped,[24] hereby providing a way toward integration of corrugated apertures in compact device architecture. Our study also demonstrates that a simple 0.5 NA water immersion objective can efficiently detect a single fluorescent molecule, hereby releasing the need for high NA microscope objectives. Another remarkable point is that the structure is insensitive to the incoming polarization direction. We believe that the present demonstration is of high relevance for the development of advanced single molecule sensing, bright single-photon sources for quantum information processing, and light emitting devices.

■ ASSOCIATED CONTENT

ⓢ Supporting Information. Fabrication procedure, experimental setup and analysis methods descriptions, raw experimental data acquired with 0.5 and 1.2 NA objectives, fluorescence enhancement characterization with a 1.2 NA objective, Stern–Volmer analysis of A647 quenching, spectral analysis of the fluorescence emission, influence of the numerical aperture for collection, image scan of a single nanoaperture, and photon antibunching experiment with a corrugated nanoaperture. This material is available free of charge via the Internet at http://pubs.acs.org.

■ AUTHOR INFORMATION

Corresponding Author
*E-mail: jerome.wenger@Fresnel.fr.

■ ACKNOWLEDGMENT

■ REFERENCES

(1) Walter, N. G.; Huang, C. Y.; Manzo, A. J.; Sobhy, M. A. *Nat. Methods* 2008, 5, 475–489.
(2) Lal, S.; Link, S.; Halas, N. J. *Nat. Photonics* 2007, 1, 641–648.
(3) Craighead, H. G. *Nature* 2006, 442, 387–393.
(4) Barnes, W. L. *J. Mod. Opt.* 1998, 45, 661–699.
(5) Bharadwaj, P.; Deutsch, B.; Novotny, L. *Adv. Opt. Photonics* 2009, 1, 438–483.
(6) Fu, Y.; Lakowicz, J. R. *Laser Photonics Rev.* 2009, 3, 221–232.
(7) Schuller, J. A.; Barnard, E. S.; Cai, W. S.; Jun, Y. C.; White, J. S.; Brongersma, M. L. *Nat. Mater.* 2010, 9, 193–204.
(8) Atwater, H. A.; Polman, A. *Nat. Mater.* 2010, 9, 205–213.
(9) Anger, P.; Bharadwaj, P.; Novotny, L. *Phys. Rev. Lett.* 2006, 96, No. 113002.
(10) Kinkhabwala, A.; Yu, Z. F.; Fan, S. H.; Avlasevich, Y.; Mullen, K.; Moerner, W. E. *Nat. Photonics* 2009, 3, 654–657.
(11) Curto, A.; Volpe, G.; Taminiau, T. H.; Kreuzer, M.; Quidant, R.; Van Hulst, N. F. *Science* 2010, 329, 930–933.
(12) Taminiau, T. H.; Stefani, F. D.; Segerink, F. B.; Van Hulst, N. F. *Nat. Photonics* 2008, 2, 234–237.
(13) Koenderink, A. F. *Nano Lett.* 2009, 9, 4228–4233.

(14) Pakizeh, T.; Käll, M. *Nano Lett.* **2009**, *9*, 2343–2349.

(15) Esteban, R.; Teperik, T. V.; Greffet, J. J. *Phys. Rev. Lett.* **2010**, *104*, No. 026802.

(16) Devilez, A.; Stout, B.; Bonod, N. *ACS Nano* **2010**, *4*, 3390–3396.

(17) Lezec, H. J.; Degiron, A.; Devaux, E.; Linke, R. A.; Martin-Moreno, L.; Garcia-Vidal, F. J.; Ebbesen, T. W. *Science* **2002**, *297*, 820–822.

(18) Genet, C.; Ebbesen, T. W. *Nature* **2007**, *445*, 39–46.

(19) Garcia-Vidal, F. J.; Martin-Moreno, L.; Ebbesen, T. W.; Kuipers, L. *Rev. Mod. Phys.* **2010**, *82*, 729–787.

(20) Martin-Moreno, L.; Garcia-Vidal, F. J.; Lezec, H. J.; Degiron, A.; Ebbesen, T. W. *Phys. Rev. Lett.* **2003**, *90*, No. 167401.

(21) Nahata, A.; Linke, R. A.; Ishi, T.; Ohashi, K. *Opt. Lett.* **2003**, *28*, 423–425.

(22) Ishi, T.; Fujikata, J.; Ohashi, K. *Jpn. J. Appl. Phys.* **2005**, *44*, L364–L366.

(23) Srituravanich, W.; Pan, L.; Wang, Y.; Sun, C.; Bogy, D. B.; Zhang, X. *Nat. Nanotechnol.* **2008**, *3*, 733–737.

(24) Laux, E.; Genet, C.; Skauli, T.; Ebbesen, T. W. *Nat. Photonics* **2008**, *2*, 161–164.

(25) Yu, N.; Fan, J.; Wang, Q. J.; Plügl, C.; Diehl, L.; Edamura, T.; Yamanishi, M.; Kan, H.; Capasso, F. *Nat. Photonics* **2008**, *2*, 564–570.

(26) Moran-Mirabal, J. M.; Craighead, H. G. *Methods* **2008**, *46*, 11–17.

(27) Lenne, P. F.; Rigneault, H.; Marguet, D.; Wenger, J. *Histochem. Cell Biol.* **2008**, *130*, 795–805.

(28) Levene, M. J.; Korlach, J.; Turner, S. W.; Foquet, M.; Craighead, H. G.; Webb, W. W. *Science* **2003**, *299*, 682–686.

(29) Chansin, G. A. T.; Mulero, R.; Hong, J.; Kim, M. J.; deMello, A. J.; Edel, J. B. *Nano Lett.* **2007**, *7*, 2901–2906.

(30) Eid, J.; Fehr, A.; Gray, J.; Luong, K.; Lyle, J.; Otto, G.; Peluso, P.; Rank, D.; Baybayan, P.; Bettman, B.; Bibillo, A.; Bjornson, K.; Chaudhuri, B.; Christians, F.; Cicero, R.; Clark, S.; Dalal, R.; Dewinter, A.; Dixon, J.; Foquet, M.; Gaertner, A.; Hardenbol, P.; Heiner, C.; Hester, K.; Holden, D.; Kearns, G.; Kong, X. X.; Kuse, R.; Lacroix, Y.; Lin, S.; Lundquist, P.; Ma, C. C.; Marks, P.; Maxham, M.; Murphy, D.; Park, I.; Pham, T.; Phillips, M.; Roy, J.; Sebra, R.; Shen, G.; Sorenson, J.; Tomaney, A.; Travers, K.; Trulson, M.; Vieceli, J.; Wegener, J.; Wu, D.; Yang, A.; Zaccarin, D.; Zhao, P.; Zhong, F.; Korlach, J; Turner, S. *Science* **2009**, *323*, 133–138.

(31) McNally, B.; Singer, A.; Yu, Z.; Sun, Y.; Weng, Z.; Meller, A. *Nano Lett.* **2010**, *10*, 2237–2244.

(32) Wenger, J.; Gérard, D.; Aouani, H.; Rigneault, H.; Lowder, B.; Blair, S.; Devaux, E.; Ebbesen, T. W. *Anal. Chem.* **2009**, *81*, 834–839.

(33) Juan, M. L.; Gordon, R.; Pang, Y.; Eftekhari, F.; Quidant, R. *Nat. Phys.* **2009**, *5*, 915–919.

(34) Rigneault, H.; Capoulade, J.; Dintinger, J.; Wenger, J.; Bonod, N.; Popov, E.; Ebbesen, T. W.; Lenne, P. F. *Phys. Rev. Lett.* **2005**, *95*, No. 117401.

(35) Wenger, J.; Gérard, D.; Bonod, N.; Popov, E.; Rigneault, H.; Dintinger, J.; Mahboub, O.; Ebbesen, T. W. *Opt. Express* **2008**, *16*, 3008–3020.

(36) Aouani, H.; Wenger, J.; Gérard, D.; Rigneault, H.; Devaux, E.; Ebbesen, T. W.; Mahdavi, F.; Xu, T.; Blair, S. *ACS Nano* **2009**, *3*, 2043–2048.

(37) Mahboub, O.; Carretero Palacios, S.; Genet, C.; Garcia-Vidal, F. J.; Rodrigo, S. G.; Martin-Moreno, L.; Ebbesen, T. W. *Opt. Express* **2010**, *18*, 11292–11299.

(38) Gérard, D.; Wenger, J.; Bonod, N.; Popov, E.; Rigneault, H.; Mahdavi, F.; Blair, S.; Dintinger, J.; Ebbesen, T. W. *Phys. Rev. B* **2008**, *77*, No. 045413.

(39) Jiao, X.; Goeckeritz, J.; Blair, S.; Oldham, M. *Plasmonics* **2009**, *4*, 37–50.

(40) Aouani, H.; Itzhakov, S.; Gachet, D.; Devaux, E.; Ebbesen, T. W.; Rigneault, H.; Oron, D.; Wenger, J. *ACS Nano* **2010**, *4*, 4571–4578.

(41) Bharadwaj, P.; Novotny, L. *Opt. Express* **2007**, *15*, 14266–14274.

(42) Bharadwaj, P.; Novotny, L. *J. Phys. Chem. C* **2010**, *114*, 7444–7447.

(43) Wenger, J.; Aouani, H.; Gérard, D.; Blair, S.; Ebbesen, T. W.; Rigneault, H. *Proc. SPIE* **2010**, *7577*, 75770J.

(44) Huang, C.; Bouhelier, A.; Colas des Francs, G.; Bruyant, A.; Guenot, A.; Finot, E.; Weeber, J.-C.; Dereux, A. *Phys. Rev. B* **2008**, *78*, No. 155407.

(45) Kozako, T.; Kadoya, Y.; Hoffmann, H. F. *Nat. Photonics* **2010**, *4*, 312–315.

(46) Popov, E.; Nevière, M.; Fehrembach, A. L.; Bonod, N. *Appl. Opt.* **2005**, *44*, 6141–6154.